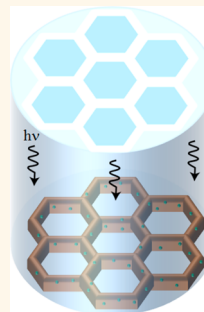


# 3D Optical Printing of Piezoelectric Nanoparticle–Polymer Composite Materials

Kanguk Kim,<sup>†,§</sup> Wei Zhu,<sup>†,§</sup> Xin Qu,<sup>‡</sup> Chase Aaronson,<sup>‡</sup> William R. McCall,<sup>‡</sup> Shaochen Chen,<sup>†,‡</sup> and Donald J. Sirbuly<sup>†,‡,\*</sup>

<sup>†</sup>Materials Science and Engineering and <sup>‡</sup>Department of NanoEngineering, University of California, San Diego, La Jolla, California 92093, United States. <sup>§</sup>K. Kim and W. Zhu contributed equally to this work.

**ABSTRACT** Here we demonstrate that efficient piezoelectric nanoparticle–polymer composite materials can be optically printed into three-dimensional (3D) microstructures using digital projection printing. Piezoelectric polymers were fabricated by incorporating barium titanate (BaTiO<sub>3</sub>, BTO) nanoparticles into photoliable polymer solutions such as polyethylene glycol diacrylate and exposing to digital optical masks that could be dynamically altered to generate user-defined 3D microstructures. To enhance the mechanical-to-electrical conversion efficiency of the composites, the BTO nanoparticles were chemically modified with acrylate surface groups, which formed direct covalent linkages with the polymer matrix under light exposure. The composites with a 10% mass loading of the chemically modified BTO nanoparticles showed piezoelectric coefficients ( $d_{33}$ ) of  $\sim 40$  pC/N, which were over 10 times larger than composites synthesized with unmodified BTO nanoparticles and over 2 times larger than composites containing unmodified BTO nanoparticles and carbon nanotubes to boost mechanical stress transfer efficiencies. These results not only provide a tool for fabricating 3D piezoelectric polymers but lay the groundwork for creating highly efficient piezoelectric polymer materials *via* nanointerfacial tuning.



**KEYWORDS:** piezoelectric · 3D printing · nanoparticle · PEG · polymer · photopolymerization

The ability to convert compressive/tensile stresses to an electric charge, or *vice versa*, has long been an intriguing and valuable property of piezoelectrics. Applications that utilize the direct (mechanical stress forming an electric field) or converse (electric voltage forming a mechanical deformation) piezoelectric effect are far reaching, ranging from loud speakers and acoustic imaging to energy harvesting and electrical actuators. Most piezoelectric materials in systems are based on brittle ceramics such as lead zirconate titanate (PZT), which has one of the highest known piezoelectric coefficients ( $d_{33} > 300$  pC/N, depending on composite and processing conditions).<sup>1</sup> Although much smaller piezoelectric responses compared to PZT, Pb-(Mg<sub>1/3</sub>Nb<sub>2/3</sub>)O<sub>3</sub>-PbTiO<sub>3</sub> (PMN-PT;  $d_{33}$  up to  $\sim 2500$  pC/N),<sup>2</sup> or other perovskite-based oxides such as barium titanate (BaTiO<sub>3</sub>, BTO;  $d_{33} > 200$  pC/N, depending on ceramic type and processing conditions),<sup>3–5</sup> piezoelectric polymer materials offer several unique capabilities that make them ideal candidates for systems that require mechanical flexibility,

smaller active elements, biocompatibility, and processability. One of the most widely studied pure polymers in this group is polyvinylidene fluoride (PVDF), discovered in 1969 by Kawai,<sup>6</sup> which has a piezoelectric coefficient ( $d_{33} \approx -20$  to  $-34$  pC/N) that is over an order of magnitude smaller than PZTs. Due to its excellent mechanical flexibility, biocompatibility, and solution-based processability, it is actively being investigated for applications including nonvolatile low-voltage memory,<sup>7</sup> acoustic transducers,<sup>8,9</sup> and implantable medical devices.<sup>10,11</sup> PVDF materials are some of the best standards when it comes to piezoelectric polymer performance, yet it is difficult to fabricate these structures into individual active elements, complex architectures, or three-dimensional (3D) patterns. Breakthroughs in the area of micro- and nanofabrication of piezoelectric polymers will have an enormous impact on the development of biodiagnostics, nano- and microelectromechanical systems, imaging, sensors, and electronics.

There are many nano- and microfabrication techniques available for ferroelectric

\* Address correspondence to dsirbuly@ucsd.edu.

Received for review June 16, 2014 and accepted July 21, 2014.

Published online July 21, 2014  
10.1021/nn503268f

© 2014 American Chemical Society

and piezoelectric materials including electron beam lithography,<sup>12,13</sup> ion milling,<sup>14,15</sup> soft lithography,<sup>16</sup> self-assembly,<sup>17</sup> electrospinning,<sup>18</sup> and contact printing.<sup>19</sup> However, these techniques do not offer simple approaches to fabricating 3D structures in piezoelectric polymers or multilayered architectures, which would open up infinite possibilities in the design of more complicated device geometries. To address the 3D printing aspect of active piezoelectric materials and pursue low-cost fabrication approaches for producing high-fidelity patterns and structures over large areas, we investigated stereolithographic (SLA) methods that use photoliable piezoelectric polymer composite materials. The general procedure for building 3D structures with SLA involves the exposure of light (typically from a laser or light-emitting diode) to a photoliable liquid (e.g., polymer solution with acrylated monomer units), which creates cross-linked regions where the light irradiates the matrix. Once a single layer is carved out with the light, the sample is translated to allow the next layer to be written. The actual patterning can be programmed with computer-aided design, but resolution is limited by actinic radiation, free radical diffusion, and the optical system, which is typically  $\sim 75$  to  $250\ \mu\text{m}$  in the  $x$ – $y$ -direction and about  $100\ \mu\text{m}$  in the  $z$ -direction.<sup>20</sup> The throughput of the SLA process is also slow due to the point-by-point scanning nature of the direct-write. To achieve higher throughput and resolutions using the basic concepts of SLA, microscale digital projection printing (DPP) can be used, which leverages a digital micromirror-array device (DMD) to produce a dynamic digital mask.<sup>21,22</sup> The projected images from the DMD are focused on the polymer solution, and feature sizes as small as  $1\ \mu\text{m}$  can be generated by sequential polymerization steps.<sup>23</sup>

In this work we describe how DPP can be utilized to photopolymerize piezoelectric nanoparticle–polymer colloidal suspensions into user-defined 2D or 3D structures in mere seconds. The piezoelectric nanoparticles are chemically modified with photosensitive surface groups and incorporated into photoliable polymer solutions. Under light exposure, the polymer cross-links with the chemical groups on the piezoelectric nanoparticles, which grafts the nanoparticles to the polymer backbones. This direct linkage to the flexible polymer matrix enhances the piezoelectric output of the composite films by efficiently funneling mechanical stress to the piezoelectric crystals. A significant boost in the piezoelectric coefficient is observed for the chemically modified nanoparticles compared to other composites with similar polymer matrices infused with carbon nanotube fillers and unmodified nanoparticles or unmodified nanoparticles alone. These results provide an immediate solution to fabricating 3D piezoelectric materials and uncover a novel strategy to enhance mechanical-to-electrical conversion in nanocomposites.

## RESULTS AND DISCUSSION

To produce 3D photowritable piezoelectric polymers, we focused on composite materials that could easily incorporate piezoelectric nanoparticles into a photoliable polymer solution. After defining a digital mask, the polymer solution can then be exposed to a pattern of light (Figure 1a) and the liquid polymerizes and encapsulates the piezoelectric nanoparticles. The system we chose for the initial work leverages BTO nanoparticles embedded in a polyethylene glycol diacrylate (PEGDA) matrix, but the platform should be universal for other photoliable polymers [e.g., poly(methyl methacrylate), poly(acrylic acid), poly(lactic acid)] and piezoelectric materials (e.g., PZT, ZnO, PMN-PT, NaNbO<sub>3</sub>). The BTO nanoparticles were synthesized using well-known hydrothermal processing that combines metal alkoxides such as Ti-butoxide [ $\text{Ti}(\text{O}(\text{CH}_2)_3\text{CH}_3)_4$ ] with metal hydroxides such as  $\text{Ba}(\text{OH})_2$  in an autoclave at  $150$ – $300\ ^\circ\text{C}$ .<sup>24</sup> The mean diameter of the synthesized nanoparticles was  $85 \pm 15\ \text{nm}$  (Figure 1b). To enhance the stress transfer efficiency from the matrix to the BTO nanoparticles and boost the piezoelectric outputs of the fabricated materials, a 3-trimethoxysilylpropyl methacrylate (TMSPM) linker molecule was used to covalently graft the BTO surface to the PEGDA matrix (Figure 1c and Figure S2 in the Supporting Information). Under light exposure the carbon–carbon double bonds of the TMSPM cross-link with the polymer matrix, forming a strong bond between the piezoelectric nanoparticles and polymer network. Compared to other piezoelectric composite materials that utilize BTO nanoparticles embedded in an elastomer [e.g., polydimethylsiloxane (PDMS)], with carbon nanotubes (CNTs) as a mechanical-to-electrical enhancer,<sup>25</sup> the direct grafting of molecular linkers provides a simpler and more efficient route to help funnel energy to the piezoelectric structures. In addition, removing the CNTs significantly improves the optical transparency of the material. Other nanocomposite polymers have been demonstrated to produce strong piezoelectric outputs without the need for additives (e.g., PDMS/PMN-PT nanowire composites),<sup>26</sup> but these utilize nanomaterials with higher intrinsic piezoelectric performance. After mixing the surface-treated BTO nanoparticles with the PEGDA solution, a photoinitiator such as 2,2-dimethoxy-2-phenylacetophenone (DMPA) or Irgacure 651 is added to generate free radicals in regions exposed to light. Once free radicals are formed, they attack the  $\text{C}=\text{C}$  bonds of the monomers in solution, producing acrylic monomers with free electrons that attack other monomers, forming oligomers and eventually a vast cross-linked network. The chain reaction propagates until two radicals neutralize or the irradiation source is turned off. For our DPP setup, the microstructure arrays were fabricated in very short times ( $<2\ \text{s}$ ), and this can be further tuned by altering irradiation power, photoinitiator concentration,

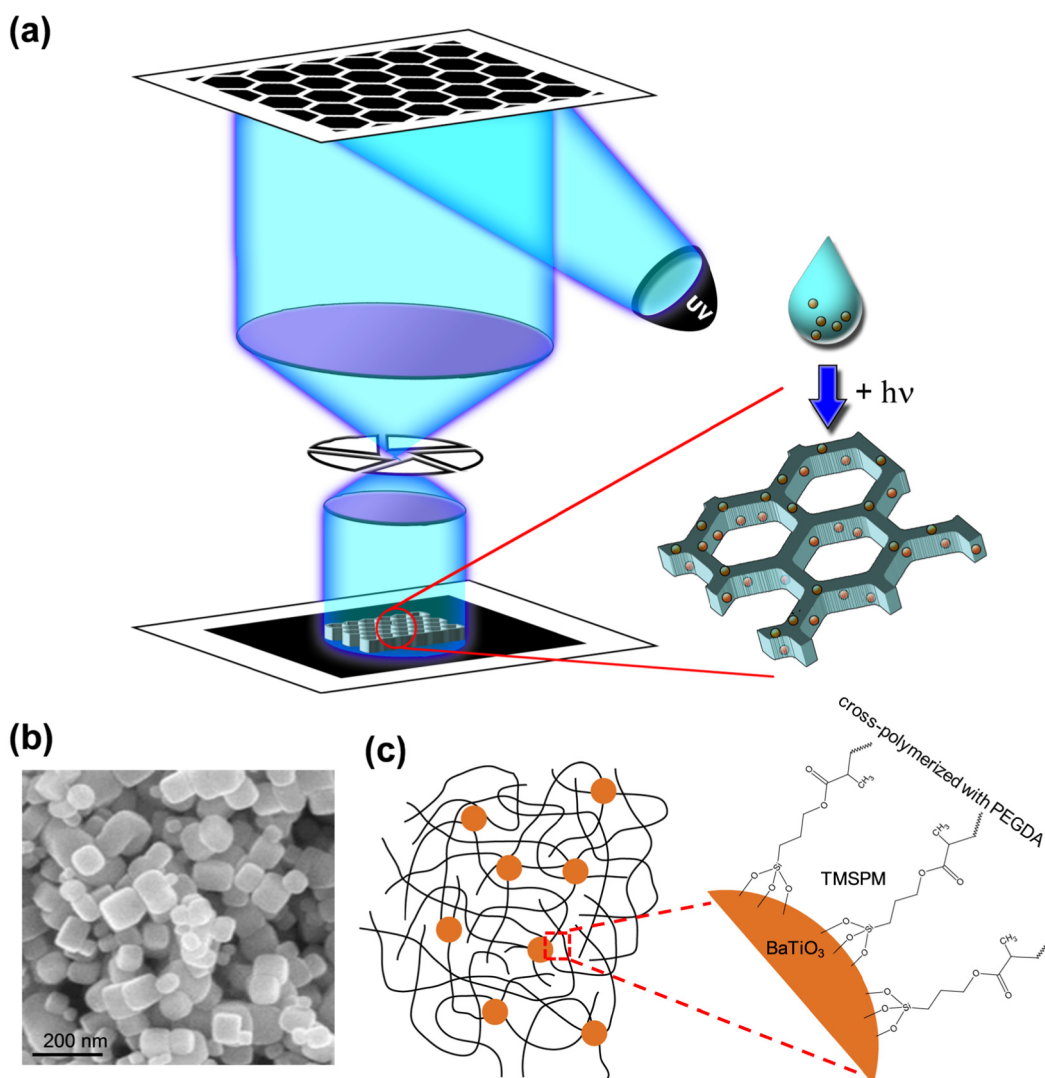


**Figure 1.** (a) Schematic of the DPP setup that projects dynamic digital masks on the photoliable piezoelectric nanoparticle–polymer composite solution. Any pattern can be digitized, and the digital mirror device projects the image onto the polymer solution. (b) Scanning electron micrograph of BTO nanoparticles grown *via* a hydrothermal process. (c) Cartoon showing the piezoelectric polymer composite materials with BTO nanoparticles (orange circles) grafted to a PEGDA matrix (black lines). The zoom-in shows the TMSPM linker covalently linked to the nanoparticle surface and cross-linked with the PEGDA matrix.

monomer concentration, or nanoparticle loading and/or adding a quencher.

With superb control over the digital photomask, virtually any shape can be projected onto the polymer solution and printed within seconds. Figure 2 shows a collage of different microstructures, including dot, square, and honeycomb arrays that were fabricated using a custom-built DPP apparatus coupled with a 365 nm light emitting diode (LED) light source. Although similar structures can be produced with other fabrication methods such as contact printing, the photoprinting process can be carried out over very large areas with high reproducibility and fidelity. In addition, there is low instrumental complexity, and the fabrication time to create batch arrays with different geometric shapes and structures can be orders of magnitude faster than techniques that require a separate mask processing step.

For 3D direct printing the stage can be translated in the z-direction (perpendicular to substrate surface) while the projected image is altered. By focusing the projected light on a plane in the liquid (or liquid surface) and synchronizing the stage movement with the incremental change in the projected features, 3D structures can be carved out with smooth side walls using a process called dynamic optical projection stereolithography (DOPsL).<sup>27</sup> Figure 3a–c shows various 3D structures created using this approach including an arbitrary mushroom-like array that has a smaller base diameter compared to the top, a cross array with a recessed center and rounded edges, and a tapered cantilever array. Creating structures with complex void regions that are layered on top of each other or features that are hollowed out will require more sophisticated photopolymerization techniques. The structures and

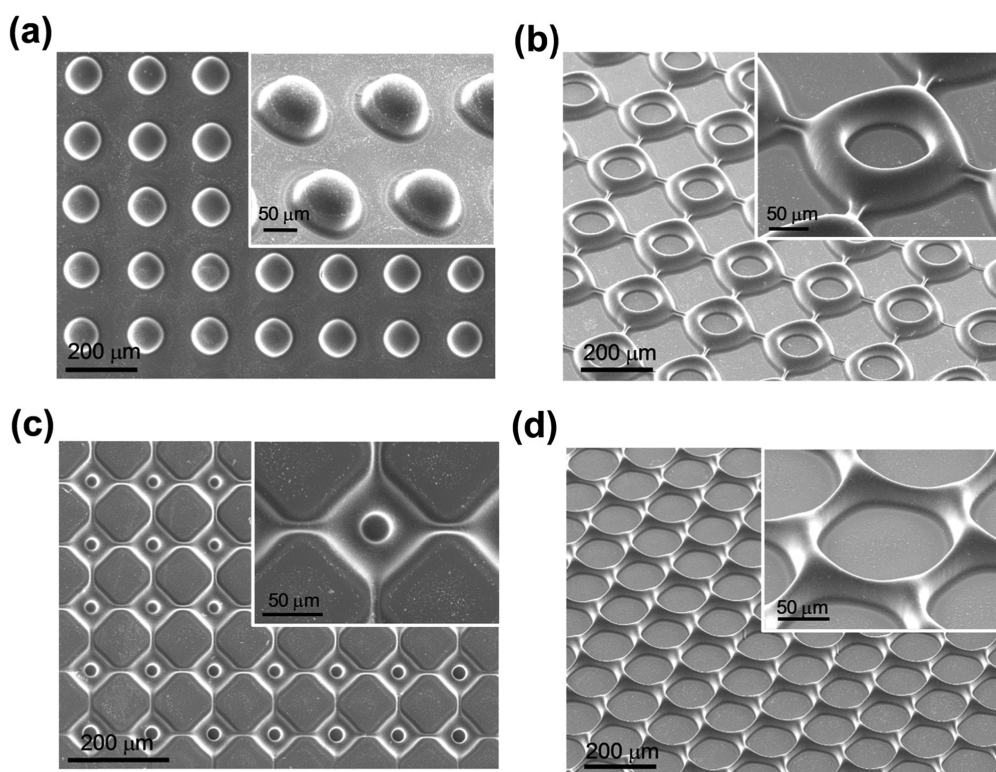


Figure 2. Collage of piezoelectric microstructures printed using DPP including (a) a dot array, (b, c) square arrays with different sized void spaces, and (d) a honeycomb array. All structures were fabricated in <2 s using a PEGDA solution loaded with 1% of the TMSPM-modified BTO nanoparticles.

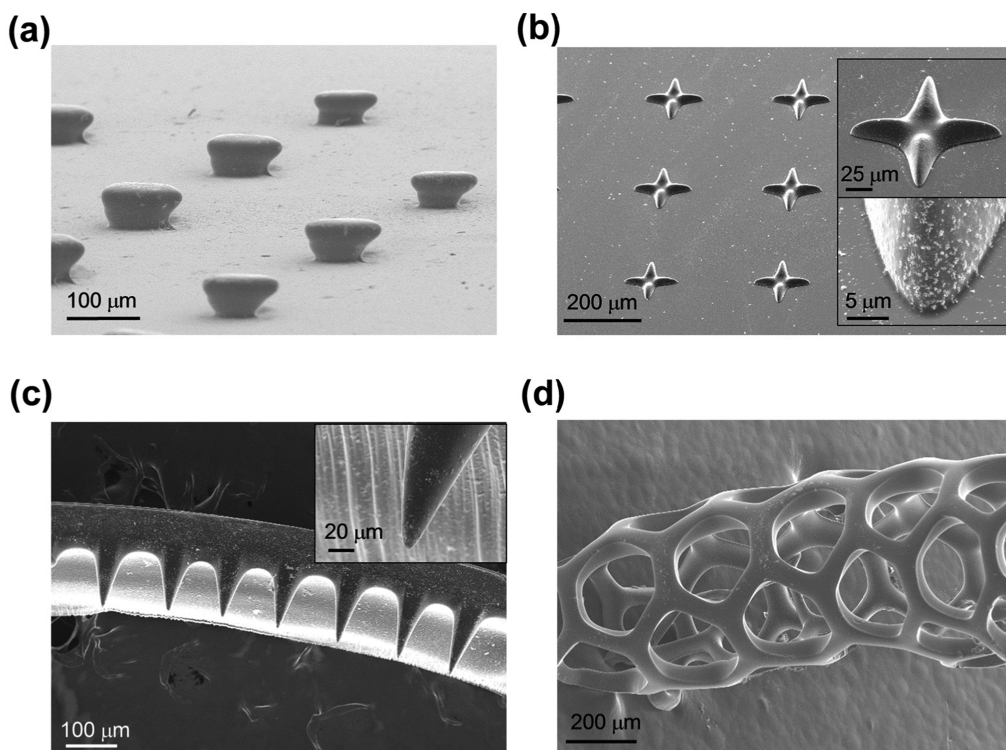


Figure 3. Various 3D structures fabricated by DOPsL including (a) a mushroom-like array, (b) a cross array, and (c) a tapered cantilever array (dark region, cantilever; light region, support). (d) Microtubule structure formed by releasing a honeycomb array from the substrate. The film rolls up after release due to slight stress gradients in the film.

arrays fabricated in Figures 2 and 3 rely on single photon absorption events to catalyze the cross-linking process. This limits how deep/thick a 2D structure is since light will be absorbed in the top layer, thereby creating free radicals well above the focal area underneath. To minimize overexposure to regions outside the focal plane, optical quenchers can be used to lower the rate of free radical formation, but the depth is still limited by attenuation of the digital mask. This can be circumvented by using DOPsL to fabricate 3D structures since the process can be designed to photopolymerize only on the top surface of the liquid. Either new polymer solutions can be flown into the reaction cell while the vertical stage is manipulated, or the polymerization can be done in sequential steps without ever having to project the digital mask through thicker ( $>5 \mu\text{m}$ ) unpolymerized layers.

The 2D and 3D patterns demonstrate the ability to reach a resolution limit of  $\sim 5 \mu\text{m}$  with curved, adjoining, straight, and/or void regions (*e.g.*, see zoom-in images in Figure 3b,c), which is close to the limit of DPP ( $\sim 1 \mu\text{m}$ ) for pure polymers. The resolution is strongly dependent on the light–matter interaction of the BTO nanoparticles. We found that BTO mass loadings of 1–10% and 1% photoinitiator produced excellent transfer efficiencies of the digital mask to the solid polymer structures while still offering strong piezoelectric outputs and similar mechanical properties to the pure PEGDA materials. As the loading goes above 10%, the transparency of the polymer goes below 5% at 365 nm, which washes out the projected mask and causes shape distortions similar to what is observed in overexposed photoresists. Extinction spectra of the BTO nanoparticles clearly show the direct relationship between light–matter interactions and the BTO concentration (Figure S3, Supporting Information). Higher loading fractions and better printing resolution should be attainable if tighter focused light sources are used, the photopolymerization wavelength is tuned so that it falls in the higher transmission (longer wavelengths) region of the colloidal polymer solution, or the nanoparticle size is reduced; all of which will be topics of future research. In addition, smaller photopolymerization spots can be created using nonlinear optical processes such as two-photon absorption (TPA); however, high laser powers are required for multiphoton processes, and the fabrication occurs *via* a much slower point-by-point scanning process.

After photofabricating the composite materials, the printing cell can be used to activate the polymer. This requires that the dipoles in the perovskite crystallites be aligned using a poling field that is larger than the coercive field ( $\sim 10 \text{ V}/\mu\text{m}$ ) of the BTO nanoparticles. This was achieved using indium tin oxide (ITO)-coated glass slides as the top and bottom electrodes, which also served as the top and bottom surface of the photofabrication cell. By placing an elastomeric spacer

(*e.g.*, PDMS or Kapton film) between the conductive glass substrates, the maximum height of the photofabricated structures is defined, and precise electric fields could be applied to polarize the BTO nanoparticles. After activating the piezoelectric composite the fabricated films can be either left on the glass slides for testing and characterization, removed to create free-standing structures, or transferred to other substrates for further integration. If the photoprinting is carried out on a substrate that has weak interactions with the PEGDA composite (*e.g.*, hydrophobic surface), the structured films can roll up to make higher order structures. The microtube shown in Figure 3d is one example where a honeycomb pattern is projected onto the nanoparticle composite solution, and after polymerization the film is removed from the substrate, which rolls up into a well-defined tubule. This process can be controlled by depositing bilayers with different thermal expansion coefficients, densities, or lattice parameters, which would govern the diameter of the tube and extent of the rolling.<sup>28</sup>

The piezoelectric properties of the photofabricated materials were investigated by applying specific loads to neat (*i.e.*, unstructured) photopolymerized films and measuring the electrical outputs with a home-built piezoelectric instrument (Figures S4 and S5, Supporting Information). Neat films were investigated to ensure robust polymer–electrode interfaces, but the patterned microstructures (*e.g.*, honeycomb array) also showed similar strong piezoelectric outputs after poling (Figure S6, Supporting Information). Loads were applied orthogonal to the substrate, and the ITO-coated glass slides were used as top and bottom electrodes. As expected, there is a significant enhancement in the cross-linked films that contain the TMSPM linker (no CNTs) compared to (1) the composite materials without the linker but with CNTs (1% by mass) or (2) the composite with BTO nanoparticles only (no CNTs or TMSPM). In fact under similar loads (1.44 N) the composite films with the grafted nanoparticles displayed a  $>2$  times boost in the piezoelectric output (Figure 4a) over the CNT composites and  $>10$  times boost over composites without CNTs or TMSPM. There was no response from films fabricated with pure PEGDA, unpolarized composite materials containing TMSPM, or unpolarized composite materials without TMSPM. Quantifying the piezoelectric response of the 10% BTO-loaded CNT composites and TMSPM-grafted composites gave effective piezoelectric coefficient ( $d_{33}$ ) values of  $13 \pm 2$  and  $39 \pm 3 \text{ pC/N}$ , respectively. These values for the composites with grafted nanoparticles are already exceeding that of pure polymers such as PVDF, which warrants further investigation into the upper limit of the photoliable composites and systematically studying the dependence of the piezoelectric properties on nanoparticle composition, polymer matrix, nanoparticle size, and linker chemistry.

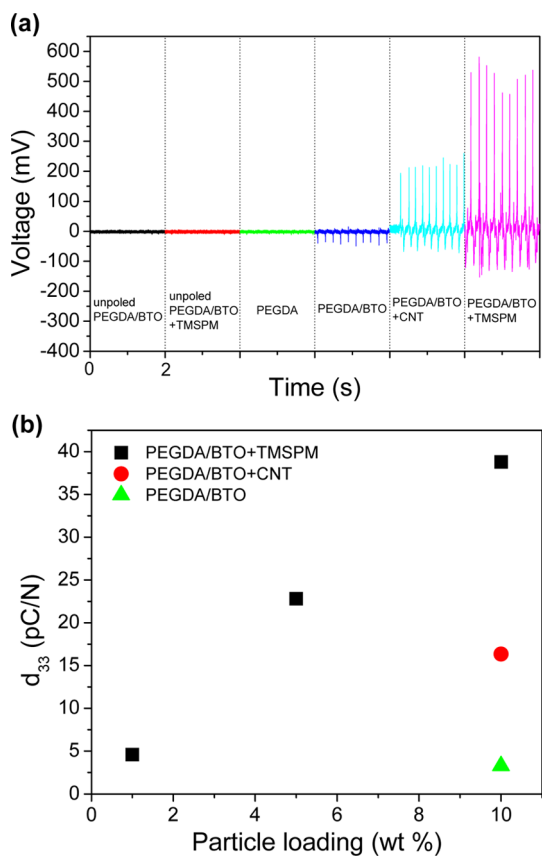


**Figure 4.** (a) Voltage response of various unpoled and poled composite materials (neat films) cycled with a 1.44 N load applied perpendicular to the surface of the film. Cycling data were collected for a total of 2 s for each film. (b) Plot showing the effective piezoelectric modulus ( $d_{33}$ ) of a grafted PEGDA/BTO composite material as a function of BTO mass loading. The piezoelectric moduli for the 10% loaded PEGDA/BTO with CNTs and PEGDA/BTO (no CNTs or TMSPM) composites are also included for comparison.

The large increase in the piezoelectric coefficient is directly related to the mechanical interface between the BTO surface and PEGDA matrix, which aids in the mechanical-to-electrical energy conversion process by efficiently funneling the stress in the polymer chains to the piezoelectric crystals. When no covalent linkages are formed between the nanoparticles and the polymer chains, the nanoparticles are just fillers and only weakly react to polymer deformations. The addition of CNTs helps stiffen the polymer matrix, which increases the mechanical response of the piezoelectric nanoparticles when the polymer chains are strained. Future studies of this BTO–polymer chemical interface will be focused on how parameters such as grafting density, linker length, and polymer type affect the piezoelectric output of the composite materials. Although the piezoelectric properties of the polymer composites are lower than those of BTO monolithic ceramics ( $\sim 200$  pC/N), the composites are performing with a much lower density of active material while maintaining their mechanical flexibility. Analyzing the piezoelectric coefficient as a function of BTO mass loading (Figure 4b)

shows a clear trend toward higher  $d_{33}$  values as the nanoparticle density increases. This upward trend should continue to increase and likely peak at a higher mass loading, but to reach the higher mass loading ( $>10\%$ ), the optical transparency of the colloidal solutions will have to be improved. There are various ways to achieve this including reducing the size of the piezoelectric nanoparticles and/or photopolymerizing with longer wavelengths. The latter can be realized using TPA techniques or photoinitiators that absorb deeper into the red/infrared regions.

## CONCLUSION

Piezoelectric materials are key components in a range of devices including acoustic imaging, energy harvesting, and actuators and typically rely on brittle ceramic monoliths to perform their functions. To control the size and or shape of the piezoelectrics, it is common to use mechanical dicing or saws. However, this limits not only the size of the piezoelectric element but also the dimensionality. It is nearly impossible with current cutting techniques to shape brittle ceramics into higher order 3D structures, which could have a huge impact on compact sensor designs, tunable acoustic arrays, efficient energy scavengers, and diagnostic devices. To address this issue, we have demonstrated a novel tool for fabricating 3D piezoelectric materials that relies on piezoelectric nanoparticles embedded in a photoliable polymer solution. Digital optical masks generated by a programmable digital mirror device can project any user-defined pattern on the solution, and in mere seconds the areas exposed to light photopolymerize, leaving a solid structure after washing away the unexposed polymer. The proof-of-concept experiments were performed with BTO colloids mixed with PEGDA solutions, but the technology can easily be translated to other piezoelectric materials and polymers.

In addition to the DPP technology for printing 3D piezoelectric polymers, we introduced a novel means of enhancing the mechanical-to-electrical conversion process of nanocomposites. By chemically modifying the surface of the piezoelectric nanoparticles with linker molecules that cross-link with the polymer matrix under light exposure, we formed direct covalent bonds with the polymer chains, which helped channel the mechanical stresses from the deformed matrix through the piezoelectric nanoparticles. This boosted piezoelectric performance by over 10 and 2 times compared to the composite fabricated without the linker molecules and those loaded with CNTs, respectively. The 3D printable resolution for the composite materials approached the  $\sim 1$   $\mu\text{m}$  limit using DPP, but this is solely governed by the light–matter interactions of the polymer solution and the spot size of the light source. Although not a focus of this work, there are various means of pushing the resolution down to

diffraction-limited sizes, which include the use of non-linear effects such as TPA and higher focusing components. Overall, these results are far reaching and should

have immediate impact on a multitude of research fields including bioengineering, materials science, physics, and chemistry.

## METHODS

**Barium Titanate Nanoparticle Synthesis.** BTO nanoparticles were synthesized by hydrothermal methods similar to those found in literature.<sup>24,29</sup> The precursors for the reaction included barium hydroxide monohydrate [Ba(OH)<sub>2</sub>·(H<sub>2</sub>O), Sigma-Aldrich, 98%], titanium butoxide [Ti(O(CH<sub>2</sub>)<sub>2</sub>CH<sub>3</sub>)<sub>4</sub>, Ti-butoxide; Sigma-Aldrich, 97%], and diethanolamine [NH(CH<sub>2</sub>CH<sub>2</sub>OH)<sub>2</sub>, DEA, Fisher Scientific, laboratory grade]. First, 25 mmol of Ti-butoxide was added to 10 mL of ethanol followed by the addition of 3.5 mL of ammonia. The Ti-butoxide solution was then mixed with the Ba-hydroxide solution, which contained 37.5 mmol of Ba-hydroxide in 12.5 mL of DI water. The DEA (2.5 mL) was then added to the solution to help control the size of the nanoparticles. The final solution was transferred to a Teflon-lined stainless steel reactor, and the reactor was kept in an oven at 200 °C for 16 h. After the reaction, the reactor was cooled to room temperature and the particles were cleaned 10 times with a vacuum filter using ethanol and DI water. The final product was dried at 80 °C for 24 h.

**Preparation of PEGDA and BTO Nanoparticle Composites.** Prior to mixing the BTO nanoparticles with the PEGDA solutions, the dried nanoparticles were functionalized with TMSPM using similar grafting strategies to those carried out on silica surfaces.<sup>30</sup> The TMSPM solution consisted of 1 mL of TMSPM dissolved in 50 mL of ethanol and was mixed with an acetic acid solution (1 mL of acetic acid in 9 mL of DI water). The BTO nanoparticles (~0.6 g) were then added to the TMSPM solution and sonicated for 24 h. After the surface functionalization step, the particles were cleaned with copious amounts of ethanol and water and dried. FTIR measurements were taken on as-made and freshly functionalized nanoparticles (Figure S2, Supporting Information). To prepare the BTO-loaded PEGDA solutions, appropriate BTO:PEGDA weight ratios were used to achieve the desired mass loading, and the samples were sonicated for >24 h prior to photopolymerization.

**Optical Printing and Film Preparation.** The optical printing cells consisted of cover glass slides coated with 100 nm of ITO deposited by magnetic sputtering. The electrodes were covered with ~1 μm of poly(methyl methacrylate) (PMMA) to prevent shorting. A photoinitiator such as DMPA or Irgacure 651 was added to the PEGDA composites at a concentration of 1 wt %. The PEGDA composite was then placed between the two electrodes using a 25 μm Kapton film or PDMS spacer, and the solution was polymerized using 365 nm light from an LED (for DPP) or a hand-held UV lamp (for film preparation). The power of the hand-held lamp was much lower than the LED, which required longer exposure times (minutes) to photopolymerize. Electrical wires were connected to the electrodes using silver epoxy, and the photopolymerized samples were electrically poled at a field of ~12 MV/m at 120 °C for 24 h. The piezoelectric properties of the polymers were characterized using a home-built charge amplifier (Figures S4 and S5, Supporting Information) and a commercially available force sensor (Tekscan, A201). The piezoelectric polymer was placed in between two PDMS pieces prior to placing on the force sensor to protect the materials during the mechanical test and to distribute the load equally over the active area of the piezoelectric.

**Conflict of Interest:** The authors declare no competing financial interest.

**Acknowledgment.** We would like to thank John Warner for his help in drawing figure schematics. This project is supported in part by grants (CMMI 1332681 and CMMI 1130894) from the U.S. National Science Foundation.

**Supporting Information Available:** Analytical and spectroscopic (XRD, FTIR, UV–vis) data, electronic diagrams of piezoelectric

test equipment, and piezoelectric output of a microstructured array are available free of charge via the Internet at <http://pubs.acs.org>.

## REFERENCES AND NOTES

- Jaffe, B.; Cook, W. R.; Jaffe, H. *Piezoelectric Ceramics*; Academic Press: London, 1971.
- Fu, H. X.; Cohen, R. E. Polarization Rotation Mechanism for Ultrahigh Electromechanical Response in Single-Crystal Piezoelectrics. *Nature* **2000**, *403*, 281–283.
- Karaki, T.; Yan, K.; Miyamoto, T.; Adachi, M. Lead-Free Piezoelectric Ceramics with Large Dielectric and Piezoelectric Constants Manufactured from BaTiO<sub>3</sub> Nano-Powder. *Jpn. J. Appl. Phys., Part 2* **2007**, *46*, L97–L98.
- Takahashi, H.; Numamoto, Y.; Tani, J.; Matsuta, K.; Qiu, J. H.; Tsunekawa, S. Lead-Free Barium Titanate Ceramics with Large Piezoelectric Constant Fabricated by Microwave Sintering. *Jpn. J. Appl. Phys., Part 2* **2006**, *45*, L30–L32.
- Wada, S.; Yako, K.; Kakemoto, H.; Tsurumi, T.; Kiguchi, T. Enhanced Piezoelectric Properties of Barium Titanate Single Crystals with Different Engineered-Domain Sizes. *J. Appl. Phys.* **2005**, *98*, 014109.
- Kawai, H. Piezoelectricity of Poly (Vinylidene Fluoride). *Jpn. J. Appl. Phys.* **1969**, *8*, 975–976.
- Hu, Z.; Tian, M.; Nysten, B.; Jonas, A. M. Regular Arrays of Highly Ordered Ferroelectric Polymer Nanostructures for Non-Volatile Low-Voltage Memories. *Nat. Mater.* **2009**, *8*, 62–67.
- Foster, F. S.; Harasiewicz, E. A.; Sherar, M. D. A History of Medical and Biological Imaging with Polyvinylidene Fluoride (PVDF) Transducers. *IEEE Trans. Ultrason., Ferroelect., Freq. Contr.* **2000**, *47*, 1363–1371.
- Harris, G. R.; Preston, R. C.; DeReggi, A. S. The Impact of Piezoelectric PVDF on Medical Ultrasound Exposure Measurements, Standards, and Regulations. *IEEE Trans. Ultrason., Ferroelect., Freq. Contr.* **2000**, *47*, 1321–1335.
- Wang, F.; Tanaka, M.; Chonan, S. Development of a PVDF Piezopolymer Sensor for Unconstrained in-Sleep Cardiorespiratory Monitoring. *J. Intell. Mater. Syst. Struct.* **2003**, *14*, 185–190.
- Lee, S.; Bordatchev, E. V.; Zeman, M. J. F. Femtosecond Laser Micromachining of Polyvinylidene Fluoride (PVDF) Based Piezo Films. *J. Micromech. Microeng.* **2008**, *18*, 045011.
- Alexe, M.; Harnagea, C.; Hesse, D.; Gosele, U. Patterning and Switching of Nanosize Ferroelectric Memory Cells. *Appl. Phys. Lett.* **1999**, *75*, 1793–1795.
- Ganpule, C. S.; Stanishevsky, A.; Aggarwal, S.; Melngailis, J.; Williams, E.; Ramesh, R.; Joshi, V.; de Araujo, C. P. Scaling of Ferroelectric and Piezoelectric Properties in Pt/SrBi<sub>2</sub>Ta<sub>2</sub>O<sub>9</sub>/Pt Thin Films. *Appl. Phys. Lett.* **1999**, *75*, 3874–3876.
- Chang, L. W.; McMillen, M.; Morrison, F. D.; Scott, J. F.; Gregg, J. M. Size Effects on Thin Film Ferroelectrics: Experiments on Isolated Single Crystal Sheets. *Appl. Phys. Lett.* **2008**, *93*, 132904.
- Nagarajan, V.; Stanishevsky, A.; Ramesh, R. Ferroelectric Nanostructures via a Modified Focused Ion Beam Technique. *Nanotechnology* **2006**, *17*, 338–343.
- Xia, Y. N.; Whitesides, G. M. Soft Lithography. *Annu. Rev. Mater. Sci.* **1998**, *28*, 153–184.
- Alexe, M.; Gruverman, A.; Harnagea, C.; Zakharov, N. D.; Pignolet, A.; Hesse, D.; Scott, J. F. Switching Properties of Self-Assembled Ferroelectric Memory Cells. *Appl. Phys. Lett.* **1999**, *75*, 1158–1160.
- Chang, C. E.; Tran, V. H.; Wang, J. B.; Fuh, Y. K.; Lin, L. W. Direct-Write Piezoelectric Polymeric Nanogenerator with High Energy Conversion Efficiency. *Nano Lett.* **2010**, *10*, 726–731.

19. Gallego-Perez, D.; Ferrell, N. J.; Higuera-Castro, N.; Hansford, D. J. Versatile Methods for the Fabrication of Polyvinylidene Fluoride Microstructures. *Biomed. Microdevices* **2010**, *12*, 1009–1017.
20. Arcaute, K.; Mann, B. K.; Wicker, R. B. Stereolithography of Three-Dimensional Bioactive Poly(Ethylene Glycol) Constructs with Encapsulated Cells. *Ann. Biomed. Eng.* **2006**, *34*, 1429–1441.
21. Han, L.-H.; Suri, S.; Schmidt, C. E.; Chen, S. Fabrication of Three-Dimensional Scaffolds for Heterogeneous Tissue Engineering. *Biomed. Microdevices* **2010**, *12*, 721–725.
22. Mapili, G.; Lu, Y.; Chen, S. C.; Roy, K. Laser-Layered Microfabrication of Spatially Patterned Functionalized Tissue-Engineering Scaffolds. *J. Biomed. Mater. Res., Part B* **2005**, *75B*, 414–424.
23. Zorlutuna, P.; Annabi, N.; Camci-Unal, G.; Nikkhah, M.; Cha, J. M.; Nichol, J. W.; Manbachi, A.; Bae, H.; Chen, S.; Khademhosseini, A. Microfabricated Biomaterials for Engineering 3D Tissues. *Adv. Mater.* **2012**, *24*, 1782–1804.
24. Chen, D. R.; Jiao, X. L. Solvothermal Synthesis and Characterization of Barium Titanate Powders. *J. Am. Ceram. Soc.* **2000**, *83*, 2637–2639.
25. Park, K.-I.; Lee, M.; Liu, Y.; Moon, S.; Hwang, G.-T.; Zhu, G.; Kim, J. E.; Kim, S. O.; Kim, D. K.; Wang, Z. L.; Lee, K. J. Flexible Nanocomposite Generator Made of BaTiO<sub>3</sub> Nanoparticles and Graphitic Carbons. *Adv. Mater.* **2012**, *24*, 2999–3004.
26. Xu, S.; Yeh, Y.-w.; Poirier, G.; McAlpine, M. C.; Register, R. A.; Yao, N. Flexible Piezoelectric PMT-PT Nanowire-Based Nanocomposite and Device. *Nano Lett.* **2013**, *13*, 2393–2398.
27. Zhang, A. P.; Qu, X.; Soman, P.; Hribar, K. C.; Lee, J. W.; Chen, S.; He, S. Rapid Fabrication of Complex 3D Extracellular Microenvironments by Dynamic Optical Projection Stereolithography. *Adv. Mater.* **2012**, *24*, 4266–4270.
28. Schmidt, O. G.; Eberl, K. Nanotechnology - Thin Solid Films Roll up into Nanotubes. *Nature* **2001**, *410*, 168–168.
29. Lee, H.-W.; Moon, S.; Choi, C.-H.; Kim, D. K. Synthesis and Size Control of Tetragonal Barium Titanate Nanopowders by Facile Solvothermal Method. *J. Am. Ceram. Soc.* **2012**, *95*, 2429–2434.
30. Du, M.; Zheng, Y. Modification of Silica Nanoparticles and Their Application in UDMA Dental Polymeric Composites. *Polym. Compos.* **2007**, *28*, 198–207.